



Towards a global investigation of transcriptomic signatures through co-expression networks and pathway knowledge for the identification of disease mechanisms

Rebeca Queiroz Figueiredo ^{1,2,†}, Tamara Raschka ^{1,2,3,†}, Alpha Tom Kodamullil ^{1,4},
Martin Hofmann-Apitius ^{1,2}, Sarah Mubeen ^{1,2,3,†} and Daniel Domingo-Fernández ^{1,3,5,*†}

¹Department of Bioinformatics, Fraunhofer Institute for Algorithms and Scientific Computing, Sankt Augustin 53757, Germany, ²Bonn-Aachen International Center for IT, Rheinische Friedrich-Wilhelms-Universität Bonn, Bonn 53115, Germany, ³Fraunhofer Center for Machine Learning, Germany, ⁴Causality Biomodels, Kinfra Hi-Tech Park, Kalamassery, Cochin, Kerala, India and ⁵Enveda Biosciences, Boulder, CO 80301, USA

Received March 18, 2021; Revised May 17, 2021; Editorial Decision June 08, 2021; Accepted June 11, 2021

ABSTRACT

We attempt to address a key question in the joint analysis of transcriptomic data: can we correlate the patterns we observe in transcriptomic datasets to known interactions and pathway knowledge to broaden our understanding of disease pathophysiology? We present a systematic approach that sheds light on the patterns observed in hundreds of transcriptomic datasets from over sixty indications by using pathways and molecular interactions as a template. Our analysis employs transcriptomic datasets to construct dozens of disease specific co-expression networks, alongside a human protein-protein interactome network. Leveraging the interoperability between these two network templates, we explore patterns both common and particular to these diseases on three different levels. Firstly, at the node-level, we identify most and least common proteins across diseases and evaluate their consistency against the interactome as a proxy for their prevalence in the scientific literature. Secondly, we overlay both network templates to analyze common correlations and interactions across diseases at the edge-level. Thirdly, we explore the similarity between patterns observed at the disease-level and pathway knowledge to identify signatures associated with specific diseases and indication areas. Finally, we present a case scenario in schizophrenia, where we show how our approach can be used to investigate disease pathophysiology.

INTRODUCTION

Despite the exponential growth of biomedical data in the last decades, we are still far from understanding the function of every gene in a living organism. Nevertheless, major technological advancements now enable us to assign specific biological functions to thousands of protein-coding genes in the human genome (1). In turn, complex interactions between groups of genes, proteins and other biomolecules give rise to the normal functioning of the cell. By acquiring knowledge of these interactions, we can decipher the molecular mechanisms which cause system-wide failures that can lead to disease (2). A common modeling approach to represent these vast sets of interactions is in reconstructing mechanisms in the form of networks as intuitive representations of biology, where nodes denote biological entities and edges their interactions (3,4).

Numerous standardized formats have been widely adopted to model biological networks that represent pathway knowledge dispersed throughout the scientific literature (5). Pathway models in a variety of formats can be found housed in databases such as KEGG (6) and Reactome (7), each with a varied focus and scope. These databases can be specifically leveraged for hypothesis generation, the analysis of biomedical data such as with pathway enrichment (8), or predictive modeling (9). Using the networks of known molecular interactions, one can also discern novel genes involved in particular disease states as functions of network proximity (10). A general trend noted by Huang and colleagues was the observation that larger networks tended to outperform smaller ones, an effect also observed when comparing the performance of integrated pathway databases to individual ones in enrichment and predictive modeling tasks (11).

*To whom correspondence should be addressed. Tel: +49 2241 14 4036; Email: daniel.domingo.fernandez@scai.fraunhofer.de

†The authors wish it to be known that, in their opinion, the first two and last two authors should be regarded as Joint First/Last Authors.

Although knowledge-driven approaches that leverage literature-based evidence can be used to gain a mechanistic understanding of disease pathophysiology, these approaches tend to be augmented when applied in combination with data-driven ones. In the latter case, transcriptomic profiling offers researchers a systematic and affordable method to analyze the expression and activity of genes and proteins on a large-scale under distinct physiological conditions. Through gene expression profiling, patterns of genes expressed at the transcript level that are relevant to a particular condition can be determined, whilst considering sets of genes involved in a specific biological process tend to exhibit similar patterns of expression or activity (12). To model these patterns, techniques such as gene co-expression networks have been developed in which genes with correlated expression activity are connected. Several methodologies can be used to generate co-expression networks, such as Weighted Gene Co-expression Network Analysis (WGCNA) (13), SWItchMiner (SWIM) (14) and ARACNE (15). Co-expression networks tend to be represented as undirected weighted graphs, where graph nodes correspond to genes, and edges between nodes correspond to co-expression relationships (16). The applications of these networks are diverse, ranging from identifying functional and disease-specific modules to hub genes (12). For instance, Chou *et al.* (17) and Xiang *et al.* (18) combined independent datasets related to endometrial cancer and Alzheimer's disease, respectively, in order to generate co-expression networks that captured gene expression patterns across multiple disease-specific datasets. Using these co-expression networks, they were able to identify relevant genes in the context of these two indications.

Though it is standard practice to perform enrichment analysis using pathway and gene set databases (e.g. KEGG and Gene Ontology (19)) on gene lists from co-expression networks such as those from a particular disease module (20,21) for mechanistic insights, this approach ignores the topology of the network as it exclusively relies upon sets of genes rather than the network structure. In a recent study, Paci *et al.* (22) overcame this challenge by showing how distinct, topological properties of disease networks can emerge through the identification and mapping of disease-specific genes of several disease co-expression networks to a human interactome network of protein-protein interactions. The SWIM method used by the authors has independently been applied to elucidate the molecular mechanisms that underlie several complex diseases mediated by the identification of key genes (23–26).

The potential insights that can be gained from the previously mentioned analyses together with the abundance of publicly available transcriptomic datasets (27,28) have prompted the creation of databases that store collections of co-expression networks, such as COXPRESdb for numerous species (29). By harmonizing and storing thousands of transcriptomic datasets in the form of co-expression networks, these resources capture a variety of ‘snapshots’ representing gene expression patterns in a diverse set of contexts. While transcriptomics datasets have been used to identify regulatory patterns across a variety of different contexts such as specific species or tissues (30), the aim of most transcriptomics data analyses is to reveal biological pro-

cesses that differentiate a disease patient from a healthy control. The large amount of datasets available contain an abundant number of samples, allowing for comprehensive large-scale analyses on a variety of indications. Furthermore, by bringing together transcriptomic data with known interactions in pathway resources, we can connect the transcriptome with the proteome by overlaying the patterns in co-expression networks with the scaffold of biological knowledge embedded in pathway networks (31). In doing so, we can gain insights on specific or shared molecular mechanisms across multiple indications.

In this work, we jointly leverage the patterns of disease-specific datasets reflected in co-expression networks and pathway and interaction networks to uncover the mechanisms underlying disease pathophysiology. To do so, we systematically compared hundreds of transcriptomic datasets from over 60 diseases with a human protein-protein interactome network to unravel the proteins, subgraphs, and pathways that are specific to certain diseases or shared across multiple. Finally, in a case scenario, we demonstrate how bringing together a disease-specific co-expression network with pathway knowledge allows us to better understand the role of a specific pathway within a disease context.

MATERIAL AND METHODS

In the first subsection, we outline the process of generating disease-specific co-expression networks from transcriptomic data (Figure 1A–C). Then, we describe the construction of a human protein-protein interactome network (Figure 1E and F). Finally, we outline the various analyses conducted (Figure 1D).

Generating co-expression networks from transcriptomic data

Identifying disease-specific datasets in ArrayExpress. We queried datasets from ArrayExpress (AE) (27) belonging to the most widely used platform: the Affymetrix Human Genome U133 Plus 2.0 Array (accession on AE: A-AFFY-44). By using the same platform for each of the datasets, we ensured that the datasets were relatively comparable. ArrayExpress was preferred over other databases such as Gene Expression Omnibus (GEO) (28) as datasets often comprise of normalized and mapped terms in their metadata that describe their characteristics (e.g. experimental details, organism information, etc.). Furthermore, it provides a user-friendly API through which all the necessary information was queried. As of 20 July 2020, 4485 datasets generated from platform A-AFFY-44 have been stored in ArrayExpress, resulting in roughly below 200 000 samples. Figure 2 summarizes the filtering steps that we conducted to identify disease-specific datasets which are also described below.

As the purpose of this work was to analyze disease-specific datasets, only patient samples and their controls were eligible for the analysis. Thus, a filtering step was introduced to focus exclusively on patient-level data (Figure 2, filter A). To filter out irrelevant datasets, we leveraged keywords present in the metadata such as ‘dose’, ‘compound’ or ‘strain’ (Figure 2, filter B). Furthermore, information about the disease state of each sample is needed for building disease-specific networks. Therefore, the metadata columns

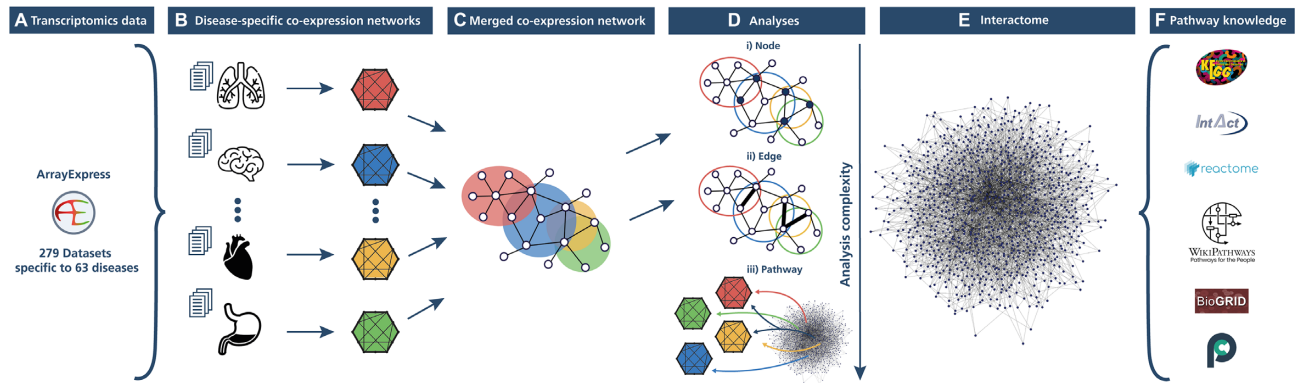


Figure 1. Schematic illustration of the methodology. 279 transcriptomic datasets were acquired from ArrayExpress (A) and grouped into 63 distinct diseases to generate disease-specific co-expression networks (B). A comprehensive protein-protein interactome network was built (E) from an ensemble of six pathway and interaction databases (F). A series of analyses were then conducted on the disease-specific co-expression networks (D), specifically: a node-level analysis (D.i), an edge-level analysis (D.ii), and a pathway-based analysis (D.iii) leveraging pathway knowledge and the interactome network.

were searched for disease keywords like ‘disease’, ‘histology’ or ‘status’ (Figure 2, filter C). This resulted in 651 datasets, of which one non-human dataset was removed, totaling in 650 datasets with 51 550 samples (Figure 2, filter D).

Once datasets were filtered to identify those that contained disease-specific information, we then harmonized the disease terms present in the title and metadata of the datasets with the help of the Human Disease Ontology (DOID) (32). Next, the disease terms from patient samples were mapped to DOID entities using ZOOMA (<https://www.ebi.ac.uk/spot/zooma>), enabling us, in some cases, to automatically find DOID matches. However, the majority of the terms did not contain a perfect match to a DOID entity so ZOOMA proposed the closest match. Based on this set of proposed DOID entities, we manually evaluated whether the term had been correctly assigned or if a DOID entity that could more accurately represent the disease was available. Through this process, we also identified false positive terms which had not been successfully filtered in the previous steps. In these cases, the metadata did not contain sufficient information, though this information was present in the dataset title. Thus, using the title information, we removed such false positive terms following manual inspection.

To maximize the coverage, we conducted a final processing step where we intended to group similar diseases together under a common label. For that, we leverage the ontology network structure and visualize it as a hierarchical tree with a focus on selected branches (i.e. ‘immune system disease’, ‘nervous system disease’, and ‘cancer’). Next, we manually identify close neighbors for terms that have few samples in order to merge them into a more general term that still accurately describes the original term. The veracity of the likeliness of the disease terms in the selected clusters to be used as a single gene expression set were verified by a clinician before re-mapping. (Supplementary Text 1).

After this final grouping step, we also filtered datasets to fulfill the following criteria: i) ensure every disease has a minimum of 50 samples to increase the stability of the co-expression network, ii) ensure a minimum of two datasets per disease, and iii) exclude samples with the ‘cancer’ la-

bel as this term was too broad (Figure 2, filter F). Thus, we have 38 621 samples from 469 datasets as 63 distinct diseases and one control group (Supplementary Table S1). To facilitate the grouping of control samples, we first harmonized all samples coming from datasets used to generate the disease networks that correspond to controls by giving them a common label (i.e. ‘normal’) (Figure 2, filter G). Applying the previously described filtering steps resulted in 35 025 samples from 323 datasets that were selected. Finally, not all datasets comprised the raw data required to generate the co-expression networks which are solely based on 279 datasets (20 748 samples) (Figure 2, filter H). The final list of datasets with their respective disease labels can be seen in Supplementary Table S1 and can be visualized according to their DOID hierarchy in Supplementary Figure S1.

Scripts to retrieve and process the datasets from ArrayExpress are available at <https://github.com/CoXPath/CoXPath/blob/main/R>. We have also provided comprehensive documentation to modify the filtering steps and add extensions to the scripts.

Generating co-expression networks. For each disease, expression data could then be used to construct co-expression networks to represent relationships between genes in different diseases. Therefore, the raw .CEL-files of the expression datasets were downloaded, pre-processed, and merged. Here, each individual dataset was first pre-processed with the RMA function of the oligo package in R, which performs background subtraction and quantile normalization. After merging the samples from different datasets irrespective of the sample tissue (as this information was not available for a large amount of samples), a batch correction via ComBat (33) was applied to the data to remove the effect corresponding to individual datasets. Finally, the probes were mapped to genes. If multiple probes mapped to the same gene, the most variable probe was kept. In the special case of the normal network, we would like to note that only control samples that were present in the disease datasets were used (Figure 2, filter G).

The actual co-expression datasets were then constructed with the WGCNA package in R (13). WGCNA has been shown to be one of the most accurate methods, even in the

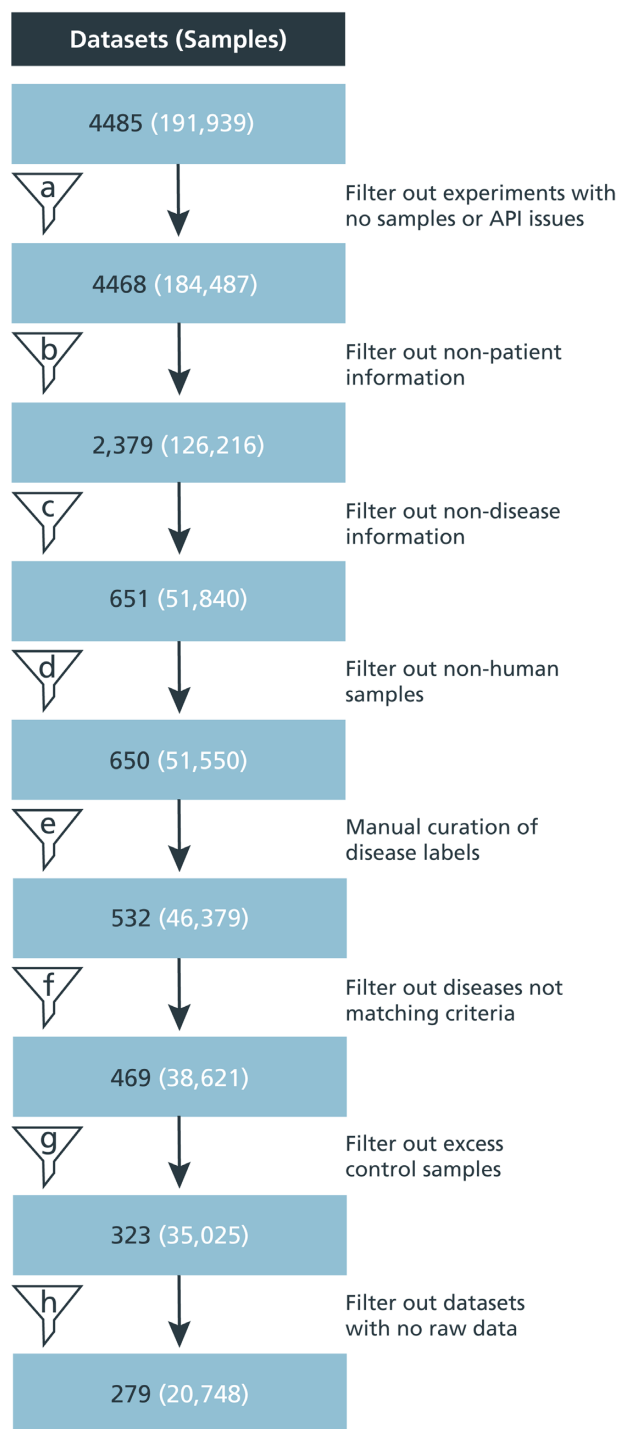


Figure 2. Extracting disease-specific datasets from ArrayExpress. transcriptomic data from nearly 4500 datasets was derived from ArrayExpress. Several filtering steps (A–H) were applied to only retain disease-specific datasets for patient samples and controls that fulfilled the criteria outlined in the section: Identifying disease-specific datasets in ArrayExpress.

case of small sample sizes, as opposed to other methods such as ARACNE (34). But, in contrast to most common approaches that construct and analyze modules of the network based on hierarchical clustering, here we relied only on the topological overlap matrix (TOM). In order to fa-

cilitate the comparability of the networks, for each disease, we defined its co-expression network as the top 1% highest similarity in the TOM as it is considered a conservative cut-off in benchmark studies (35) and enables us to maintain the same number of edges in each network while the number of nodes can vary. Nodes having a higher topological overlap were previously found to be more likely to belong to the same functional class than nodes having lower topological overlap (36). Given the platform used in this study (i.e. Affymetrix Human Genome U133 Plus 2.0 Array), 1% corresponds to 2 036 667 edges for each co-expression network. This cut-off for connections with the highest topological overlap was used because without a stringent cut-off, we would yield fully connected networks of over 200 million edges. However, since most of the genes do not have such a high topological overlap, the majority of these edges would not be relevant for our analysis as they would have a weight close to zero (see Supplementary Text 2 for more details). Finally, we would like to mention that we refer to these edges interchangeably as correlations through this paper. Although this is not precise, edges representing a high topological overlap are also highly correlated as the TOM value is based on the signed correlation but also takes the connectedness of nodes into account.

Building a human protein–protein interactome network

To systematically compare disease-specific co-expression networks against pathway knowledge, we built an integrative network comprising information from a compendium of well-established databases. This interactome was comprised of tens of thousands of human protein–protein interactions from six databases including KEGG (6), Reactome (7), WikiPathways (37), BioGrid (38), IntAct (39) and PathwayCommons (40). We would like to note that the first three of the six databases were harmonized through PathMe (41). Additionally, for each of the six databases, only proteins that belonged to pathways from MPath (11), an integrative resource that combines multiple databases and merges gene sets of equivalent pathways, were included in the interactome, thus ensuring that each protein in the network was minimally assigned to a single pathway. The use of MPath to annotate proteins to pathways facilitated both the generation of a larger network and the avoidance of redundant pathways.

The resulting human interactome has a total of 8601 nodes and 199 535 edges. Not surprisingly, the vast majority of the nodes in the interactome are protein-coding genes, as these genes are transcribed into functional proteins with essential roles in the biological processes represented in pathway databases (Figure 3A). Among the edges of the interactome, association relations are the most prevalent (~73%), while causal relations including, increase, decrease, regulate, and has_component relations constitute the remaining relation types (Figure 3B). Apart from the interactome network we generated, we also obtained protein–protein interactions (PPIs) from HIPPIE (42) and STRING (43) to compare the results yielded by our network containing pathway knowledge with other comprehensive PPI resources. Unlike the protein–protein interactome, the STRING and HIPPIE networks were not constrained to only contain pro-

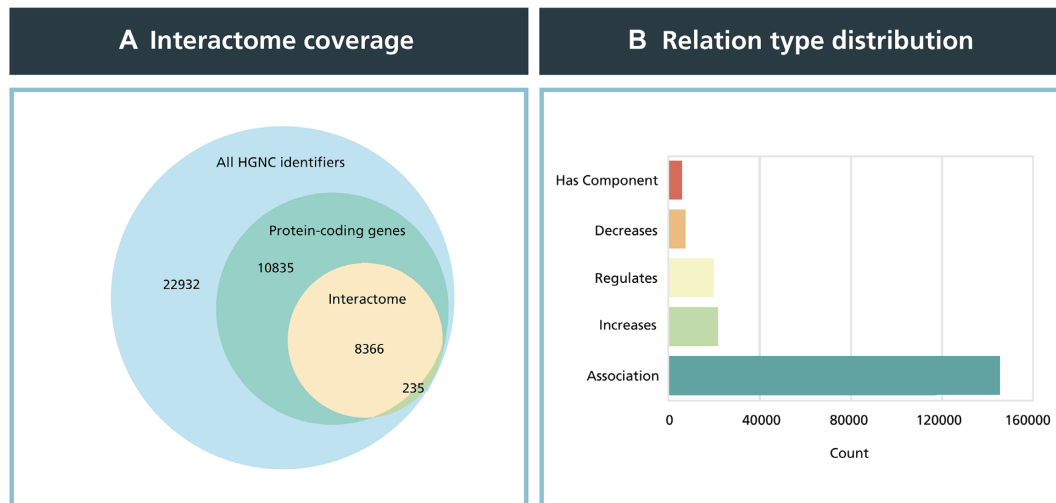


Figure 3. Node and edge type statistics of the human protein-protein interactome network. (A) Venn diagram indicating the coverage of proteins in the interactome network with respect to all existing HGNC identifiers as well as protein-coding genes. The interactome contains ~8600 unique HGNC identifiers, or 20% of the roughly 42 300 approved HGNC identifiers. In total, 97% of the HGNC identifiers of the interactome are protein-coding genes. (B) Distribution of relation types in the interactome network. The largest proportion of relation types were associations, comprising nearly 73% of all ~200 000 edges, while causal relations, specifically decrease, regulate, and increase, made up ~25% of all relation types with roughly 50 000 edges.

teins which could be annotated to pathways. Thus, both networks contained a significantly greater number of proteins and PPIs (detailed descriptions of these networks can be found in Supplementary Table S2).

Analyses

Software and data used in network analysis and visualization. Network analyses were conducted using the methods and algorithms implemented in NetworkX (v2.5) (44). KEGG pathways (6) were downloaded on 3 August 2020 using ComPath (41). Network visualizations were done using WebGL, D3.js, and Three.js and the python-igraph package. The processed data and analyses are available at <https://github.com/CoXPath/CoXPath>.

Meta-analysis of gene expression data. Differential expression analysis was performed using the Limma R package (45) on the merged disease datasets previously described which contained information on both patient samples and controls. This step yielded differentially expressed genes (DEGs) for 46 diseases in total from the original 63. For all other diseases, no matching control data was available (Supplementary Table S3). For example, both datasets (E-GEOD-13141 and E-GEOD-16237) used to build the neuroblastoma dataset only consisted of neuroblastoma samples. DEGs for each disease were then filtered to include only those with an adjusted P -value < 0.05 . DEGs across the 46 diseases were combined into a consensus by splitting the up- and down-regulated genes for each disease and taking the average adjusted P -values and \log_2 fold changes for all up- and down-regulated subsets separately.

Quantifying the similarity between disease-specific co-expression networks and biological pathways. To investigate the consensus between the patterns present in each co-expression network and pathway knowledge,

we superimposed each disease-specific co-expression network against pathways from KEGG and the interactome network using two different methods. Method 1 investigates every pairwise combination of nodes from the set of proteins P for a given pathway from KEGG (C_P) to find the proportion of edges that exist in the disease co-expression network $D = (P', E_D)$ between those node pairs, namely edge overlap (edge overlap = $|\{\forall e_{u,v} \text{ s.t. } u, v \in C_P; u, v \in P' \text{ and } e_{u,v} \in E_D\}|$) (Equation 1). P' is the set of proteins in the co-expression network and E is the set of edges connecting the proteins.

$$\text{pathway-based similarity } (P, D) = \frac{\text{edge overlap}}{|C_P|} \quad (1)$$

Equation 1. Similarity between a pathway and disease co-expression network using method 1.

Similarly, applying a more stringent criterion to take into account the protein-protein interactome network, using a set of proteins P for a given pathway from KEGG, method 2 takes the interactome network $I = (U, E_i)$ and generates a subgraph $S = (V, E_S)$ containing only those nodes in P with edges in E_i (with $V = \{u : e_{u,v} \in E_S \text{ and } u, v \in P \cap U\}$ and $E_S = \{e_{u,v} : u, v \in P; u, v \in U; e_{u,v} \in E_i\}$). Next, the proportion of edges on the interactome subgraph S that are also found in each disease co-expression network $D = (P', E_D)$ are calculated (Equation 2).

$$\text{interactome-based similarity } (P, D) = \frac{|E_S \cap E_D|}{|E_S|} \quad (2)$$

Equation 2. Similarity between a pathway and disease co-expression network using method 2.

We would like to mention that we exclusively used pathway definitions (i.e. gene sets) from KEGG which contain a relatively fewer number of pathways in order to facilitate the interpretation of the analysis (e.g. Reactome contains

over 2000 pathways while KEGG has over 300). Nonetheless, in method 2, we overlay the KEGG gene sets onto the interactome network, ensuring that the analysis is not only restricted to biological interactions in KEGG.

Pathway enrichment analysis. Overrepresentation analysis (ORA) was conducted employing a one-sided Fisher's exact test (46) for each of the pathways in KEGG (downloaded on 12 December 2020). A pathway is considered to be significantly enriched if its adjusted *P*-value is smaller than 0.05 after applying multiple hypothesis testing correction using the Benjamini–Yekutieli method (47).

RESULTS

In the first subsection, we outline the diseases that fulfilled the criteria to generate the corresponding co-expression networks and investigate the characteristics of these networks. Then, we analyze the disease-specific co-expression networks at the node- and edge- levels, respectively, while later comparing the co-expression networks against pathway knowledge. Finally, in a case scenario we demonstrate how a pathway-level analysis in a disease context can be leveraged to better understand the role of a specific pathway in a disease context.

Overview of disease-specific co-expression networks

From over 330 datasets that were categorized into distinct diseases, we systematically constructed 64 co-expression networks, 63 of which correspond to disease-specific co-expression networks, and the remaining corresponding to a control group co-expression network. Figure 4A summarizes the network size of each disease-specific co-expression network clustered by major disease indication for a total of ten disease categories and one unspecific group. Body system clusters (e.g. gastrointestinal system disease, immune system disease) were given priority for the classification of all cancers before considering the 'other cancer' group. How each disease relates to its disease category cluster can be visualized on the DOID hierarchy in Supplementary Figure S1. The sarcoma co-expression network had the least number of nodes of all the networks (i.e. 5450), while the ductal carcinoma in situ co-expression network had the highest number of nodes (i.e. 20 163). Generally, the networks within each disease category cluster tended to vary greatly in size. For example, the 'immune system disease' category includes networks ranging in size from 5754 to 18 449 nodes. Additionally, the number of co-expression networks within a disease cluster varied, with nearly half the disease groups containing between 6 and 15 networks (i.e. gastrointestinal system disease, immune system disease, nervous system disease, respiratory system disease, and other cancer), while all remaining clusters contained less than five.

We also investigated whether a correlation exists between the number of samples or datasets used to create a co-expression network and the size of the network. No dependency of network size based on the amount of samples/datasets used was observed (Supplementary Figure S2). The total number of datasets ranged from 1 to

27, while the total number of samples was between 9 and 2515. The vast majority of disease co-expression networks were generated from 1 to 10 datasets and contained between 9 to 461 samples. We found that the resulting network size for each disease varied within a wide range (i.e. between ~6000 and 20 000) and no discernible pattern was observed.

Investigating global trends of disease-specific co-expression networks at the node level

Exploring the most and least common proteins of the co-expression networks. Here, we explored the most and least common proteins across all 63 disease-specific co-expression networks generated with the goal of identifying both disease-specific and commonly occurring proteins. We first identified the most common proteins as those that occur in the highest number of disease co-expression networks (Supplementary Figure S3). We discovered that 96–99% of the top 1000 to top 100 most common disease proteins, in intervals of 100, are also found in the normal network, indicating that these proteins are widespread and therefore not disease-associated proteins. Additionally, we found that none of the proteins were present in all co-expression networks as we were only interested in considering the top 1% strongest correlations in each network (i.e. the selected cut-off; see Generating co-expression networks section). On the other hand, TXLNGY and NCR2 were the most common proteins, occurring in 60 out of the 63 disease co-expression networks. Nonetheless, we were able to identify 48 proteins present in at least 57 of the 63 diseases.

We next assessed the overlap between all proteins of the interactome and the disease co-expression networks (Supplementary Figure S4). From this overlap, we investigated whether proteins in the disease co-expression networks could consistently be identified in our interactome network to infer how well these proteins have been studied and reported in the literature. We refer to proteins that could consistently be found across the majority of disease co-expression networks and were also present in the interactome as the most common proteins of the disease networks and the most highly connected proteins of the interactome. Surprisingly, we found that only 30–33.4% of the most common proteins (with cut-offs between 50 and 54 out of 63) of the disease co-expression networks were present in the interactome. Similarly, for an approximately proportional range of these most common disease proteins against the most connected proteins of the interactome (i.e. top 100–400 proteins), little to no overlap was observed (Supplementary Figure S5). We also found that the average number of relations for the proteins in the interactome that overlapped with the approximately top 400 most common proteins in the disease networks (~33 relations) was lower than the average number of relations overall in the interactome (~46 relations). This analysis was also conducted on networks built using the STRING and HIPPIE PPI resources; relative to the interactome, we found a much larger overlap between proteins in these networks and proteins of the disease co-expression networks (Supplementary Figures S6 and S7). Within these overlaps, we observed similarly small overlaps of the most com-

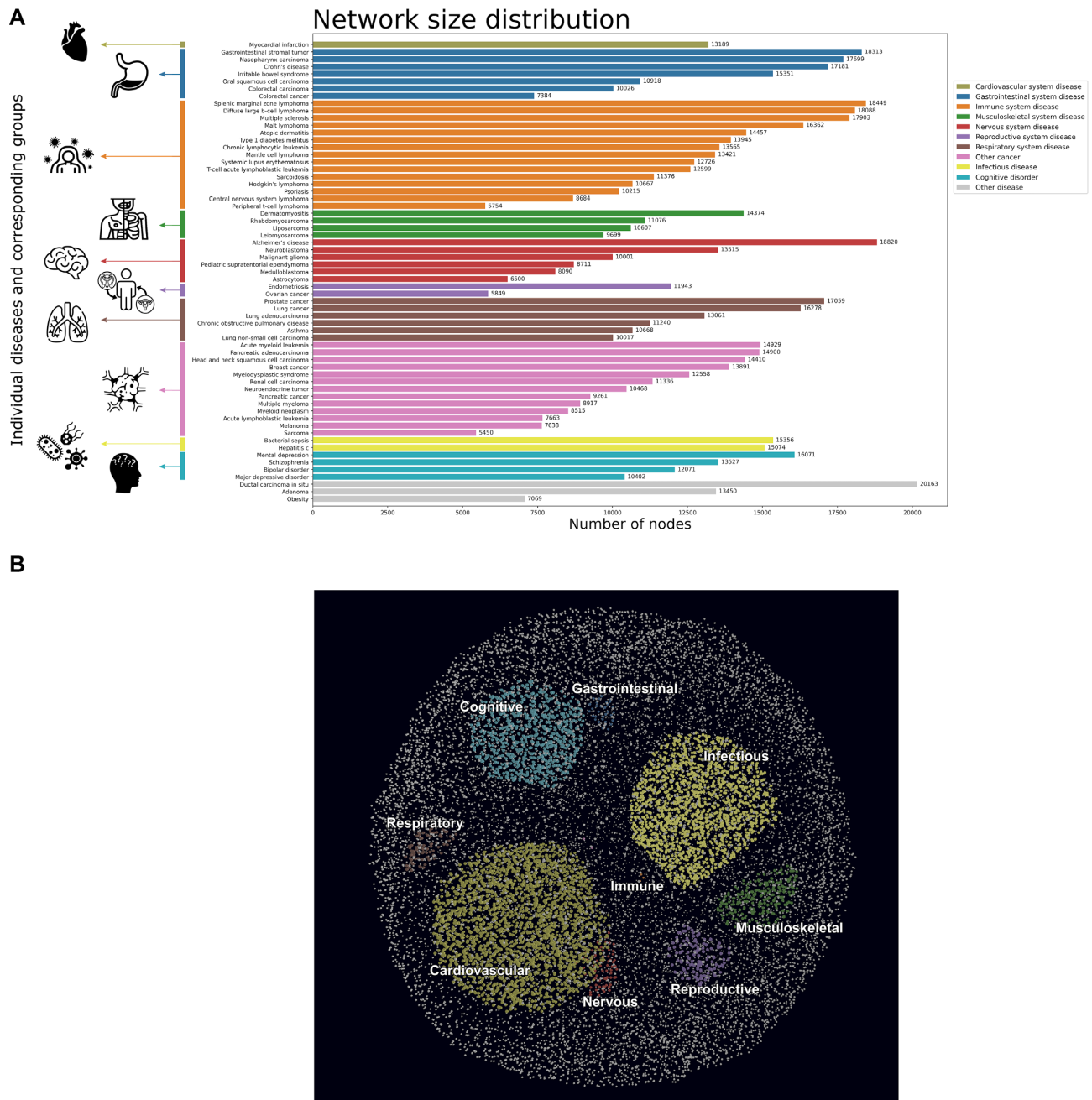


Figure 4. (A) Overview of the size of each of the co-expression networks clustered by major disease groups. **(B)** Merged co-expression network clustering proteins by their association to different disease groups. In A) each of the 63 diseases was grouped into one of ten categories (or a remaining leftover group). Here, we see the varied sizes of co-expression networks within their corresponding disease clusters. In B) association was determined by selecting the set of nodes which were present in all of the diseases of a given disease cluster (excluding 'other' and 'other cancer'), and eliminating those nodes which were also present in all diseases of other clusters. This resulted in unique sets of nodes which were guaranteed to be found in all diseases of the given cluster, but not in all of another cluster. As expected, we observed an inverse correlation between the number of diseases in a cluster and the size of the associated node subset. High quality versions are available at <https://github.com/CoXPath/CoXPath/tree/main/results/figures>.

mon disease proteins and the most connected proteins of these two networks (Supplementary Figures S8 and S9). We then evaluated the overlap between all proteins from KEGG pathways and the disease co-expression networks (Supplementary Figure S10) and sought to verify whether the most common proteins in the disease co-expression networks could also be found in pathway databases. In doing

so, we identified only a small proportion (i.e. 29–31%) of these proteins in KEGG (Supplementary Table S4). When comparisons were made against KEGG pathway annotations, we observed that these few most common proteins had, on average, a slightly lower number of pathway annotations (~14.8) than the average number of annotations for all proteins in the pathway database (~16). Taken to-

gether, these findings indicate that though these proteins are the most common across all disease co-expression networks, they tend to be underrepresented in the scientific literature.

Among the proteins in common between the top 400 most highly connected proteins of the interactome and the most common proteins in the disease co-expression networks, 13 proteins, including three members of the cytochrome P450 family of enzymes (i.e. CYP1A2, CYP2C9 and CYP3A4), a major ribosomal protein (i.e. RPL18), as well as key regulatory proteins such as CDK1, PRKCG and PLCB2 were present in the overlap (Supplementary Table S4 and Supplementary Figure S6). Similarly, we define proteins that could be consistently found across the majority of disease co-expression networks and were also present in KEGG pathway annotations as the most common proteins of the disease networks and the most common KEGG proteins. We examined the overlap between the top 400 most common disease proteins with the highest number of KEGG pathway annotations, and the most common proteins of the disease co-expression networks (Supplementary Figure S11). Among the 22 proteins in common, we found seven members of the human leukocyte antigens (HLA) system of proteins (HLA-B, HLA-C, HLA-DMA, HLA-DMB, HLA-DQB1, HLA-DRA and HLA-G), as well as several proteins which were also in the overlap between the aforementioned most highly connected proteins of the interactome and most common proteins in the disease co-expression networks (i.e. CAMK2A, ELK1, GNAO1 and PLCB2) (Supplementary Table S4 and Supplementary Figure S11).

Finally, we investigated the least common proteins in the disease co-expression networks and their overlap with those in the interactome, additional PPI resources and pathway knowledge (Supplementary Figures S12–S15). Similar to the most common ones, we found that the majority of the least commonly occurring proteins in the co-expression networks were not present in the interactome nor in KEGG, suggesting that little is currently known of these proteins. Among the least commonly occurring proteins that overlapped with proteins from both KEGG and the interactome, we observed a significant number of proteins from the ZNF family (i.e. 42/54 (78%) from KEGG and 12/43 (28%) from the interactome overlap) (Supplementary Table S4). This family is one of the largest protein families and is known to regulate a wide range of biological processes, while some of its members have already been associated with several disorders (48). Thus, it may be interesting to investigate proteins that are specific to a particular disease, or a few distinct diseases, in detail. As an example, we observed that TWIST1, one of the least commonly occurring proteins and a well-known oncogene (49), was exclusively present in only 25 diseases and over 50% of them were cancers (Supplementary Table S4 and Supplementary Figure S15).

Meta-analysis on consistently differentially expressed genes across diseases. Differential gene expression analysis was performed in order to pinpoint genes which were consistently significantly differentially expressed between patient and control samples across 46 diseases. While here, we in-

dependently conducted the meta-analysis to identify patterns of dysregulation among DEGs that are specific to or shared across diseases, in the case scenario we demonstrate how DEGs can be overlaid with disease-specific co-expression networks and the interactome to elucidate mechanisms that DEGs may be involved in. The average of all genes in these diseases that were up-regulated as well as the average of all genes that were down-regulated were independently calculated. Figure 5 jointly reports the comparison of the negative \log_{10} adjusted P -values versus \log_2 fold changes of all independently averaged up- and down-regulated DEGs in the 46 diseases. We found that nearly all genes were, to some degree, up-regulated in one or more diseases and down-regulated in at least one other, while only CCDC43, JADE3, RPL22L1, SOCS1 and TOR3A were exclusively up- and CAVIN2 and ZSCAN18 down-regulated across all diseases they were present in. In all, nearly 20 000 unique genes were significantly differentially expressed (adjusted P -value < 0.01), with ~ 17 600 up-regulated DEGs and ~ 15 600 down-regulated ones.

We then applied a \log_2 fold change threshold of 1.75 to identify significantly (adjusted P -value < 0.01) differentially expressed genes with the most extreme average \log_2 fold change values. This threshold was selected as it yielded a reasonable number of DEGs to investigate (i.e. 60), whereas more commonly used thresholds, such as \log_2 fold change > 1.5 , yielded over 200. Among the genes that were found to be significantly differentially expressed at the extremes, 34 were the most up-regulated and 26 were the most down-regulated (Supplementary Table S5).

These genes were then compared to the top 500 most and least common disease proteins. Of the genes that were the most up-regulated, CDK1 was also among the top 500 most common disease proteins, while CRNDE, DEPTOR, and RASD1 were among the 500 least common. Similarly, for genes that were the most down-regulated, only S100A8 was among the top 500 most common disease proteins while no genes overlapped with the 500 least common disease proteins. Additionally, we found that four of the most up-regulated genes belonged to the collagen group of protein (i.e. COL11A1, COL1A1, COL1A2 and COL3A1), while some protein families (i.e. S100 protein family, SLC, and SYNP) could be found both in the most up- and down-regulated genes.

Of the most significantly highly up- and down-regulated genes (i.e. adjusted P -value < 0.01 ; \log_2 fold change > 1.75), we examined their expression changes in each of the individual diseases they were involved in. Interestingly, we found a group of genes (i.e. AMPD1, BEX5, DEPTOR, IGF1, JCHAIN, MARC2, MTUS1 and NDFIP2) that were highly up-regulated in only two of nearly 20 diseases they were in (i.e. myeloid neoplasm and multiple myeloma, grouped in the other cancers cluster), and down-regulated in nearly all of the remaining. Thus, although these genes were down-regulated in the vast majority of diseases they were involved in, they still appeared among the most significantly highly up-regulated genes since they are significantly up-regulated in the two aforementioned cancers. This trend has been documented for DEPTOR, with low expression of the gene observed in most cancers, yet high overexpression seen in a group of multiple

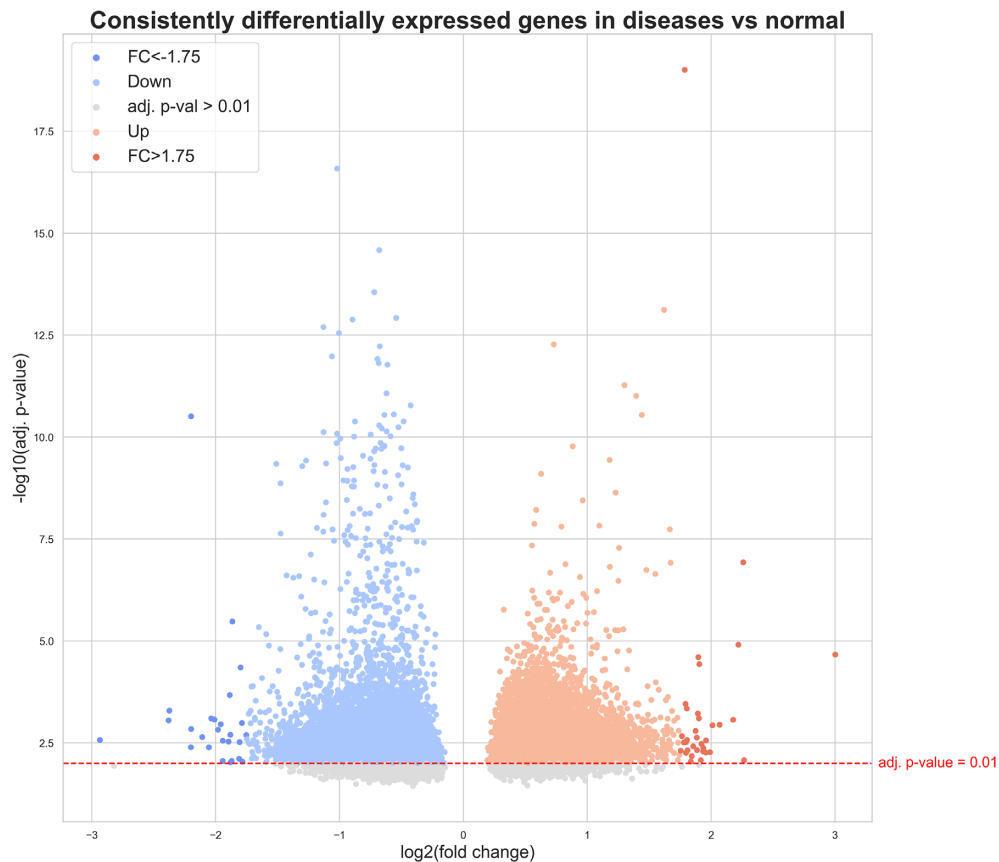


Figure 5. Consensus for consistently differentially expressed genes. Genes for 46 diseases were split into two subsets: those that were up-regulated and those that were down-regulated in that disease. The average consensus was taken for all up- and down-regulated subsets separately and is shown here. Nearly all genes could be found in both the up-regulated and down-regulated consensus as most genes are up-regulated in at least one disease as well as down-regulated in at least one other disease. In total, 19 666 unique genes were significantly up- or down-regulated (i.e. adjusted P -value < 0.01; above red line). Of the significantly differentially expressed genes, 17 643 genes were up-regulated and 15 634 genes were down-regulated. The most significantly differentially expressed genes were defined as additionally having a \log_2 fold change > 1.75, resulting in 26 most down-regulated genes (dark blue) and 34 most up-regulated genes (dark orange).

myelomas (50). Similarly, among the genes highly down-regulated, we identified a subset of genes (i.e. *ASH1L-AS1*, *CXCL8*, *DUSP4*, *EPC1*, *PANK2*, *PCIF1*, *PHLDA1* and *PMAIP1*) that were only highly down-regulated in peripheral T-cell lymphoma, whilst being up-regulated in nearly all of the remaining diseases they were in (i.e. 17 diseases on average). This pattern has been identified with the over-expression of *DUSP4*, a tumor suppressor, in certain cancer types (51), whereas the loss of its expression caused by epigenetic dysregulation has been observed in at least one type of lymphoma (52). Finally, the meta-analysis revealed that one gene with significantly highly down-regulated, *SLC8A1*, was only significantly down-regulated in a group of nervous system diseases (i.e. medulloblastoma, pediatric supratentorial ependymoma, malignant glioma, astrocytoma, and to a lesser degree, Alzheimer's disease), not altogether surprising as the *SLC8* gene family of sodium-calcium exchangers, which includes *SLC8A1*, have been shown to play important regulatory roles in the control of central nervous system functions (53). In contrast, *SLC8A1* was only identified as significantly up-regulated in multiple myeloma.

Investigating global trends of disease-specific co-expression networks at the edge level

In this subsection, we explored the most commonly occurring edges among the co-expression networks from all diseases and compared them against the normal co-expression network and the interactome. We hypothesized that the edges most common across disease networks involve the dysregulation of key proteins such as transcription factors, common edges present across several diseases as well as in the normal co-expression network correspond to non-specific interactions, and common edges which could also be identified in the interactome represent known molecular interactions.

We first assessed whether there were any edges specific to particular disease networks, identifying 57 774 118 unique edges in total (i.e. 45% of all edges). This was to be expected, as we exclusively focused on the 1% strongest correlations from the initial hundreds of millions of possible edges, which led to most of the edges in our resulting co-expression networks to be specific to a single disease. Although this unique, disease-specific set of edges are worth exploring, due to the considerably large number of edges

in the co-expression networks, we restricted our analysis to the most common edges in the co-expression networks. We found that 21 edges were in more than 70% of the diseases (44/63) and 202 in more than 50% of the diseases (32/63). Interestingly, of those 21 edges that were in 70% of the diseases, we observed that 6 of the 13 proteins which are encoded by genes in the Y chromosome appeared in 5 edges each (i.e. RPS4Y1, USP9Y, DDX3Y, KDM5D, EIF1AY and TXLNGY). Additionally, we found that nearly half of these 21 edges involved a protein of the Metallothionein family (i.e. MT1H, MT2A, MT1HL1, MT1X and MT1G), involved in the regulation of transcription factors and in cancers (54).

The most common edges in the disease co-expression networks were then compared to the normal co-expression network to identify correlations between the two, assuming that proteins involved in these edges would have basal levels of expression and that they may not be relevant to a disease-specific context. We perform a range of comparisons on the most common edges by focusing on only the top 1000 to the top 10 000, in intervals of 1000. In order to maintain a balance in these comparisons, given the high number of edges in the normal network, we subset the edges of the normal network to an equal number of edges that is currently being compared. To do so, we sort the edges of the normal co-expression network by strongest correlations (i.e. highest absolute value of weight) and select subsets of edges from the top of the list for comparison. When the most common edges in the disease co-expression networks were compared to a proportionate range of edges with the strongest correlations in the normal network (i.e. from 1000 to 10 000 edges), we found that between 19% and 17% of the edges consistently overlapped, respectively. Focusing on these ~19% of edges that were shared between the normal and most common disease networks, we were then interested in investigating whether these edges could also be found in the interactome, STRING network, and HIPPIE network. In the interactome, we found an overlap of only 8%, with this number decreasing to 4% as the number of edges being compared in disease against normal co-expression networks increased (i.e. between the top 1,000 and 10,000 most common edges). With STRING, its overlap with edges shared between the disease and normal networks was 30%, increasing to 45%, and in HIPPIE, the overlap was consistently 8%. These findings are expected because the overlap is proportional to network size (i.e. the STRING network has 20 times more edges than the interactome while HIPPIE has twice as many). Additionally, from these 8% to 4% of edges which overlapped with the interactome, we looked at the top 10 most connected proteins, consistently identifying the same proteins as the number of edges in the comparison increased. Furthermore, we found that the direct overlap between the top 1000 most common edges of the disease networks with the interactome was only 4%, 57% with the STRING network, and 6% with the HIPPIE network; while the overlap between just the top 1000 most common edges of the disease networks which were not among the top edges of the normal network with the interactome was 2%, with the STRING network 54%, and with the HIPPIE network 5%. Because this latter group of edges represents the top edges of the disease co-expression networks (but not of

the normal) which overlap with the interactome and other PPI networks, they may also warrant further investigation as they are more likely to consistently appear across diseases than in normal networks.

Overlaying co-expression networks with pathway knowledge supports the identification of disease associated pathways

In this subsection, we systematically overlaid pathway knowledge with disease co-expression networks to reveal the consensus and/or differences between the latter group of networks and well-established protein-protein interactions in pathway databases. Given that strongly co-expressed genes can be used as a proxy for functional similarity (22), it can be inferred that genes that are co-expressed could also be involved in the same pathway. In other words, we assume that if a given pathway is relevant to a disease, the proteins in the pathway would be strongly correlated in the disease co-expression network. Thus, following this assumption, we were interested in identifying the pathways associated with each of the investigated diseases. Using pathways from KEGG, we applied two methods which, i) map pathway knowledge to disease co-expression networks and ii) map pathway knowledge to the interactome, and the mapped portion of the interactome to disease co-expression networks (**see Methods**).

As expected, we noted that the results of both methods were nearly identical, indicating that pathway proteins were readily mappable to the interactome. Nonetheless, we found that the second method resulted in generally higher similarity values as it only considered edges that were identifiable in the interactome, rather than edges resulting from all possible combinations of pathway proteins (Supplementary Figure S16). Overall, clearly noticeable patterns were discernible, with groups of pathways showing variable levels of similarity in specific diseases and disease clusters (Figure 6).

In particular, we observed multiple diseases/disease clusters with higher similarity values for pathways relevant to the given disease/cluster. Among these clusters, a large group of pathways showed a high degree of similarity to cognitive disorders (Figure 6; teal), including pathways for long-term potentiation, multiple neurotransmitter systems (i.e. serotonergic synapse, glutamatergic synapse, and dopaminergic synapse), long-term depression, alcoholism, and pathways for addictions (i.e. nicotine addiction, amphetamine addiction, morphine addiction, and cocaine addiction) (Supplementary Table S6). Not surprisingly, the pathway for long-term depression showed the highest similarity with the co-expression network for mental depression. Furthermore, the gastrointestinal system disease cluster (Figure 6; blue) contained co-expression networks with the highest level of similarity with several pathways, e.g. the pathways responsible for renal cell carcinoma, colorectal cancer, pathogenic *Escherichia coli* infection, intestinal immune network for IgA production, and inflammatory bowel disease (Supplementary Table S7). Additionally, a broad group of pathways showed the highest similarity values for the two reproductive system diseases (i.e. endometriosis and ovarian cancer) (Figure 6; purple) over all other diseases and disease clusters (Supplementary Table S8). Interest-

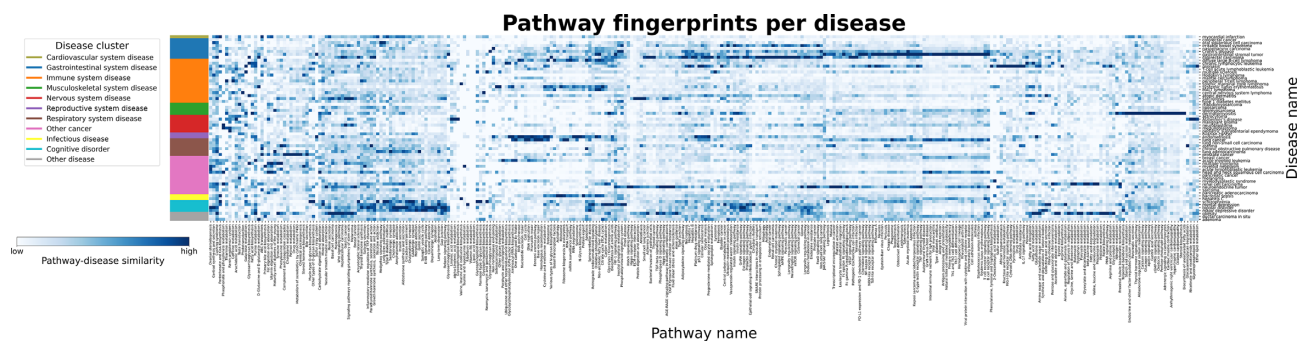


Figure 6. Mapping disease-specific expression patterns with pathway knowledge via network similarity. The heatmap illustrates the consensus similarity between KEGG pathways and disease co-expression networks. Similarity was defined as the percent of neighbors existing in a disease co-expression network out of all possible pairs of proteins from KEGG pathways (i.e. pathway-disease similarity), with lighter values corresponding to a lower similarity and darker values corresponding to higher similarity. The values (given as the percent of neighbors found) were standardized to a feature range from 0–1 for each pathway and pathways with similar values were grouped together. To ease the identification of patterns of pathway fingerprints across similar diseases, diseases were grouped by the previously defined clusters (Figure 4). A high quality version of this figure is available at <https://github.com/CoXPath/CoXPath/tree/main/results/figures>.

ingly, we found that several cancers, including gastrointestinal stromal tumor, lung cancer, head and neck squamous cell carcinoma, neuroendocrine tumor, hepatitis C, breast cancer, and ductal carcinoma in situ shared a common pattern of similar pathways (Supplementary Table S9). Among the diseases, dermatomyositis was particularly distinguishable above all others, displaying notably higher similarity to several pathways (Supplementary Table S10).

Altogether, we have demonstrated how by overlapping pathway knowledge to disease-specific co-expression networks, we can identify pathways associated with a particular disease. Additionally, we have also shown how this approach can be used to cluster diseases by the pathways they have in common, pointing to sets of potentially shared mechanisms across diseases.

Case scenario: in-depth investigation of the long-term potentiation pathway in the context of schizophrenia

In the previous section, we identified disease-associated pathways by calculating similarity between pathway knowledge and disease co-expression networks. To understand the mechanisms that underlie the similarity of a pathway to a given disease, in a case scenario, we next investigated the long-term potentiation (LTP) pathway which had yielded high similarity to the schizophrenia co-expression network. An association between this pathway and schizophrenia has already been reported in the literature, with evidence indicating impairment of LTP in the disorder (55,56).

The LTP pathway is categorized as a nervous system pathway in KEGG, with 35 edges between a set of 25 proteins/protein complexes (Figure 7). As 19 of the nodes are protein complexes containing multiple proteins, the pathway covers a total of 67 unique proteins. By overlaying the co-expression network for schizophrenia with this pathway, we identified four major edges in common, all of which were well-established interactions within this particular pathway and formed a subgraph. These edges were among the most essential of the LTP pathway; interactions between protein kinase A and the NMDA receptor, Ca^{2+} /calmodulin-dependent protein kinase II (CAMKII)

and calmodulin, and the subsequent activation of AMPAR (57) and metabotropic glutamate receptors (58) by CAMKII play key roles in determining the strength of synaptic transmission and ultimately the expression of LTP (59).

Interestingly, by overlaying the schizophrenia co-expression network with the LTP pathway, we found 53 unique correlations between proteins of the LTP pathway, indicating that the vast majority of proteins in this pathway were correlated in the co-expression network (Figure 7; grey edge), and demonstrating that indeed, proteins that are correlated in a given co-expression network can also be involved in the same biological process (31). 19 of these correlations were between calcium voltage channel complexes or calmodulin, which both have roles in the initial activation of the pathway, and other proteins (e.g. glutamate receptors). Similarly, there were approximately 20 correlations between all glutamate receptors present in the pathway and other proteins. The remaining correlations involved Erk/MAP kinase and cAMP, which ultimately regulate EP300 and CREBBP (which form the CREB binding protein complex) as well as ATF4. ATF4 is a transcription factor with multiple regulatory functions and whose polymorphisms have been associated with schizophrenia in male patients (60).

Lastly, we attempted to pinpoint candidate downstream pathways of LTP in the context of schizophrenia by investigating the edges of ATF4 given its role as a key regulator of the LTP pathway (61). As ATF4 is strongly correlated with 70 other proteins in the co-expression networks, we conducted a pathway enrichment analysis as a proxy to reveal pathway crosstalks mediated by this protein (see Methods). This analysis pinpointed four pathways from which three were involved in protein and RNA processing (i.e. ubiquitin mediated proteolysis, RNA transport, spliceosome), biological processes which have been linked with schizophrenia (62,63), while the fourth pathway, cell cycle, has also been associated with the disease (64,65) (Supplementary Table S11). These findings indicate that there may be crosstalk between these pathways that could be explored in the future.

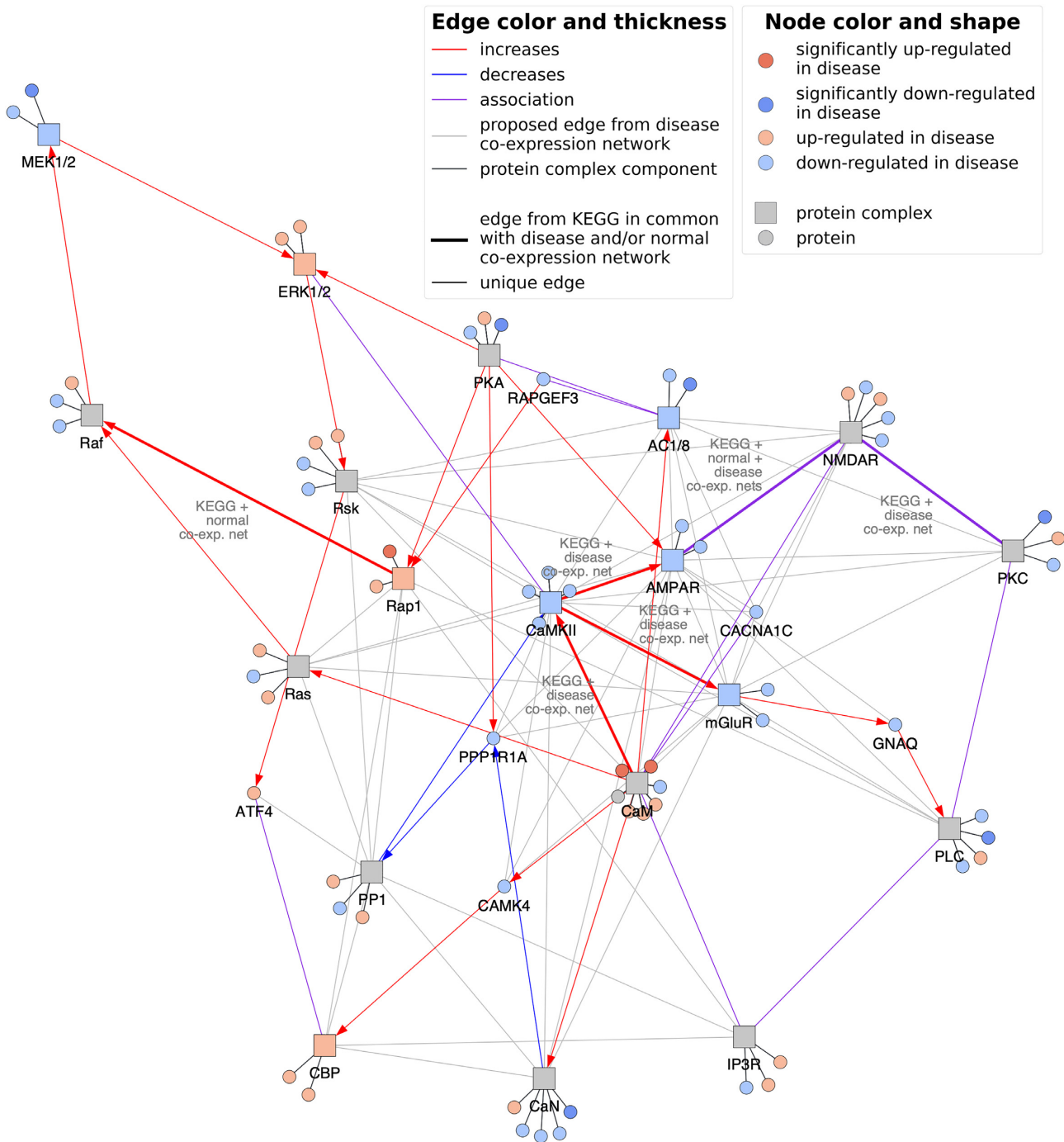


Figure 7. Long-term potentiation (LTP) pathway in the context of schizophrenia. The figure depicts the overlap of the LTP pathway with the schizophrenia co-expression network in addition to the normal co-expression network. Protein-protein interactions and associations between proteins and/or protein complexes are displayed as colored edges, while black edges denote membership of proteins to protein complexes. Edges that were common to both the LTP pathway, the disease co-expression network and/or the normal co-expression network are bolded, while grey edges denote correlations exclusively from the schizophrenia co-expression network. Differential gene expression analysis was performed and genes that were up- and down-regulated are colored orange and blue, respectively, with those that were significantly differentially expressed (i.e. adj. P value < 0.05) given less transparency. Protein complex nodes are then additionally colored if all members are in agreement with the direction of regulation. The code to generate this figure for any combination of disease co-expression network and pathway can be found at <https://github.com/CoXPath/CoXPath/blob/main/analysis/3.5.analysis.ipynb>.

DISCUSSION

Here, we have presented a systematic network-based approach that builds a bridge between disease signatures and pathway knowledge to better understand human pathophysiology. Our analysis has enabled us to globally evaluate the consensus between disease-specific transcriptomic data and an integrative human interactome network. Leveraging hundreds of transcriptomic datasets from over 60 major indications, we have explored the expression patterns observed in their corresponding co-expression networks at three different scales (i.e. at the node, edge and pathway levels). At each of these scales, we have investigated which proteins, subgraphs, and pathways could be associated with both disease-specific and shared mechanisms. Finally, we have presented a case scenario where we demonstrated how our approach can be used to investigate the role of a specific pathway in a disease-specific context.

There exist several limitations to this study. Firstly, we sought to improve the quality of the data by systematically integrating transcriptomic datasets from the same disease group, however, in doing so, we assumed that these datasets were equivalent. Although we attempted to address this assumption by enforcing a conservative inclusion and exclusion criteria as well as extensively curating the metadata associated with each dataset to group datasets into distinct diseases, disease heterogeneity for patients cannot be ignored. Secondly, we restricted this study to the most used platform in ArrayExpress in order to avoid possible effects caused by the array type, thus limiting the number of datasets that could potentially be used. Thirdly, since the cut-off chosen to generate the co-expression networks influences the resulting network (36), we exclusively focused on the 1% strongest correlations. While this cut-off was well-suited for our large-scale approach, in the future, less restrictive cut-offs could be used to generate co-expression networks as well as other methods. For instance, Pardo-Diaz *et al.* (66) recently presented a novel method that adds directionality into the co-expression network. Finally, while we constructed a human interactome network from multiple pathway and interaction databases, the majority of proteins from the co-expression networks could not be mapped to the network, highlighting the incompleteness of the current interactome.

Although we have demonstrated a proof-of-concept of our methodology across hundreds of datasets and in over sixty indications, we were only able to scratch the surface of the possible analyses that could be conducted with the resources generated within the context of this work. Thus, we have made the datasets and scripts generated in this study public to allow other researchers to conduct additional analyses on them. In the following, we outline several future applications and extensions of this work. Firstly, while we employed data from microarray technologies, the presented analysis could be expanded and/or validated by incorporating datasets generated from other platforms and technologies (e.g. RNASeq) or deposited in other databases such as GEO (28) which, in turn, can facilitate the discovery of novel genes as well as allow us to add new indications and validate the current mechanisms identified in our analysis, respectively. However, conducting such an analy-

sis would require extensive harmonization efforts at both the data and metadata level given the differences across chips and technologies, and the lack of structured metadata present in transcriptomic experiments. Secondly, the disease-specific co-expression networks generated in this work could be compared against well-established databases such as DisGeNet (67) and OMIM (68) to propose novel gene-disease associations that can be integrated into these resources. Thirdly, other advanced network analysis methods could be conducted to analyze specific network motifs in the future. Fourthly, with prior enrichment of the presented networks with drug-target information, network-based drug discovery methods can be applied to identify candidate drugs and druggable pathways for the particular disease condition(s) (69–72). Finally, another potential line of research would be to apply our methodology on datasets generated from a variety of cell lines to identify cell-specific transcriptional patterns.

DATA AVAILABILITY

All data supporting the conclusions of this article are available at <https://doi.org/10.5281/zenodo.4700652> and all scripts can be found at <https://github.com/CoXPath/CoXPath>.

SUPPLEMENTARY DATA

Supplementary Data are available at NAR Online.

ACKNOWLEDGEMENTS

We would like to thank Sumit Madan for his help running the ZOOMA queries, Carlos Bobis-Álvarez for his assistance grouping similar indications, Chris W. Diana, Helena Hermanowski and Carina Steinborn for their assistance generating the figures, and Daniel Rivas-Barragan for his valuable feedback.

Authors contributions: M.H.A. conceived the original idea. D.D.F. designed and supervised the study with assistance from SM. T.R. implemented the pipeline to download, process and categorize the gene expression datasets. R.Q.F. and T.R. generated the co-expression networks for each group. S.M. and D.D.F. generated the interactome network. R.Q.F. performed the analyses. R.Q.F., T.R., S.M. and D.D.F. interpreted the results. A.T.K., M.H.A. and D.D.F. acquired the funding. R.Q.F., T.R., S.M. and D.D.F. wrote the manuscript.

All authors have read and approved the final manuscript.

FUNDING

Fraunhofer Cluster of Excellence ‘Cognitive Internet Technologies’; German Federal Ministry of Education and Research (BMBF) [01ZX1904C]. Funding for open access charge: Institute for Algorithms and Scientific Computing. *Conflict of interest statement.* D.D.F. received salary from Enveda Biosciences.

REFERENCES

- UniProt Consortium (2019) UniProt: a worldwide hub of protein knowledge. *Nucleic Acids Res.*, **47**, D506–D515.
- Caldera, M., Buphamalai, P., Müller, F. and Menche, J. (2017) Interactome-based approaches to human disease. *Curr. Opin. Syst. Biol.*, **3**, 88–94.
- Franzese, N., Groce, A., Murali, T.M. and Ritz, A. (2019) Hypergraph-based connectivity measures for signaling pathway topologies. *PLoS Comput. Biol.*, **15**, e1007384.
- Winterbach, W., VanMieghem, P., Reinders, M., Wang, H. and deRidder, D. (2013) Topology of molecular interaction networks. *BMC Syst. Biol.*, **7**, 90.
- Hanspers, K., Riutta, A., Summer-Kutmon, M. and Pico, A.R. (2020) Pathway information extracted from 25 years of pathway figures. *Genome Biol.*, **21**, 273.
- Kanehisa, M., Furumichi, M., Sato, Y., Ishiguro-Watanabe, M. and Tanabe, M. (2021) KEGG: integrating viruses and cellular organisms. *Nucleic Acids Res.*, **49**, D545–D551.
- Jassal, B., Matthews, L., Viteri, G., Gong, C., Lorente, P., Fabregat, A., Sidiropoulos, K., Cook, J., Gillespie, M., Haw, R. *et al.* (2020) The reactome pathway knowledgebase. *Nucleic Acids Res.*, **48**, D498–D503.
- Reimand, J., Isserlin, R., Voisin, V., Kucera, M., Tannus-Lopes, C., Rostamianfar, A., Wadi, L., Meyer, M., Wong, J., Xu, C. *et al.* (2019) Pathway enrichment analysis and visualization of omics data using g:Profiler, GSEA, Cytoscape and EnrichmentMap. *Nat. Protoc.*, **14**, 482–517.
- Segura-Lepe, M.P., Keun, H.C. and Ebbels, T.M. (2019) Predictive modelling using pathway scores: robustness and significance of pathway collections. *BMC Bioinformatics*, **20**, 543.
- Huang, J.K., Carlin, D.E., Yu, M.K., Zhang, W., Kreisberg, J.F., Tamayo, P. and Ideker, T. (2018) Systematic evaluation of molecular networks for discovery of disease genes. *Cell Syst.*, **6**, 484–495.
- Mubeen, S., Hoyt, C.T., Gemünd, A., Hofmann-Apitius, M., Fröhlich, H. and Domingo-Fernández, D. (2019) The impact of pathway database choice on statistical enrichment analysis and predictive modeling. *Frontiers in Genetics*, **10**, 1203.
- vanDam, S., Vösa, U., vanderGraaf, A., Franke, L. and deMagalhães, J.P. (2018) Gene co-expression analysis for functional classification and gene–disease predictions. *Brief. Bioinform.*, **19**, 575–592.
- Langfelder, P. and Horvath, S. (2008) WGCNA: an R package for weighted correlation network analysis. *BMC Bioinformatics*, **9**, 559.
- Paci, P., Colombo, T., Fiscon, G., Gurtner, A., Pavesi, G. and Farina, L. (2017) SWIM: a computational tool to unveiling crucial nodes in complex biological networks. *Sci. Rep.*, **7**, 44797.
- Margolin, A.A., Nemenman, I., Basso, K., Wiggins, C., Stolovitzky, G., DallaFavera, R. and Califano, A. (2006) ARACNE: an algorithm for the reconstruction of gene regulatory networks in a mammalian cellular context. *BMC Bioinformatics*, **7**, S7.
- Stuart, J.M., Segal, E., Koller, D. and Kim, S.K. (2003) A gene-coexpression network for global discovery of conserved genetic modules. *Science*, **302**, 249–255.
- Chou, W.C., Cheng, A.L., Brotto, M. and Chuang, C.Y. (2014) Visual gene-network analysis reveals the cancer gene co-expression in human endometrial cancer. *BMC Genomics*, **15**, 300.
- Xiang, S., Huang, Z., Wang, T., Han, Z., Christina, Y.Y., Ni, D., Huang, K. and Zhang, J. (2018) Condition-specific gene co-expression network mining identifies key pathways and regulators in the brain tissue of Alzheimer's disease patients. *BMC Med. Genet.*, **11**, 115.
- Gene Ontology Consortium. (2019) The gene ontology resource: 20 years and still GOing strong. *Nucleic Acids Res.*, **47**, D330–D338.
- Mao, Y., Nie, Q., Yang, Y. and Mao, G. (2020) Identification of co-expression modules and hub genes of retinoblastoma via co-expression analysis and protein-protein interaction networks. *Mol. Med. Rep.*, **22**, 1155–1168.
- Yao, Q., Zhenyu, S., Wang, B. and Qin, Q. (2019) Identifying key genes and functionally enriched pathways in sjögren's syndrome by weighted gene Co-Expression network analysis. *Front. Genet.*, **10**, 1142.
- Paci, P., Fiscon, G., Conte, F., Wang, R.S., Lorenzo, F. and Loscalzo, J. (2021) Gene co-expression in the interactome: moving from correlation toward causation via an integrated approach to disease module discovery. *NPJ Syst. Biol. Appl.*, **7**, 3.
- Falcone, R., Conte, F., Fiscon, G., Pecce, V., Sponziello, M., Durante, C., Farina, L., Filetti, S., Paci, P. and Verrienti, A. (2019) BRAF V600E-mutant cancers display a variety of networks by SWIM analysis: prediction of vemurafenib clinical response. *Endocrine*, **64**, 406–413.
- Fiscon, G., Conte, F., Licursi, V., Nasi, S. and Paci, P. (2018) Computational identification of specific genes for glioblastoma stem-like cells identity. *Sci. Rep.*, **8**, 7769.
- Fiscon, G., Conte, F. and Paci, P. (2018) SWIM tool application to expression data of glioblastoma stem-like cell lines, corresponding primary tumors and conventional glioma cell lines. *BMC Bioinformatics*, **19**, 103–121.
- Paci, P., Fiscon, G., Conte, F., Licursi, V., Morrow, J., Hersh, C., Cho, M., Castaldi, P., Glass, K. and Silverman, E.K. (2020) Integrated transcriptomic correlation network analysis identifies COPD molecular determinants. *Sci. Rep.*, **10**, 3361.
- Athar, A., Füllgrabe, A., George, N., Iqbal, H., Huerta, L., Ali, A., Snow, C., Fonseca, N.A., Petryszak, R., Papatheodorou, I. *et al.* (2019) ArrayExpress update—from bulk to single-cell expression data. *Nucleic Acids Res.*, **47**, D711–D715.
- Edgar, R., Domrachev, M. and Lash, A.E. (2002) Gene Expression Omnibus: NCI gene expression and hybridization array data repository. *Nucleic Acids Res.*, **30**, 207–210.
- Obayashi, T., Kagaya, Y., Aoki, Y., Tadaka, S. and Kinoshita, K. (2019) COXPRESdb v7: a gene coexpression database for 11 animal species supported by 23 coexpression platforms for technical evaluation and evolutionary inference. *Nucleic Acids Res.*, **47**, D55–D62.
- Doncheva, N.T., Palasca, O., Yarani, R., Litman, T., Anthon, C., Groenen, M.A.M., Stadler, P.F., Pociot, F., Jensen, L.J. and Gorodkin, J. (2021) Human pathways in animal models: possibilities and limitations. *Nucleic Acids Res.*, **49**, 1859–1871.
- Vella, D., Zoppis, I., Mauri, G., Mauri, P. and DiSilvestre, D. (2017) From protein-protein interactions to protein co-expression networks: a new perspective to evaluate large-scale proteomic data. *EURASIP J. Bioinformatics Syst. Biol.*, **2017**, 6.
- Schriml, L.M., Mitraka, E., Munro, J., Tauber, B., Schor, M., Nickle, L., Felix, V., Jeng, L., Bearer, C., Lichenstein, R. *et al.* (2018) Human Disease Ontology 2018 update: classification, content and workflow expansion. *Nucleic Acids Res.*, **47**, D955–D962.
- Johnson, W.E., Li, C. and Rabinovic, A. (2007) Adjusting batch effects in microarray expression data using empirical Bayes methods. *Biostatistics*, **8**, 118–127.
- Allen, J.D., Xie, Y., Chen, M., Girard, L. and Xiao, G. (2012) Comparing statistical methods for constructing large scale gene networks. *PLoS One*, **7**, e29348.
- Perkins, A.D. and Langston, M.A. (2009) Threshold selection in gene co-expression networks using spectral graph theory techniques. *BMC Bioinformatics*, **10**, S4.
- Yip, A.M. and Horvath, S. (2007) Gene network interconnectedness and the generalized topological overlap measure. *BMC Bioinformatics*, **8**, 22.
- Martens, M., Ammar, A., Riutta, A., Waagmeester, A., Slenter, D.N., Hanspers, K., Miller, R.A., Digles, D., Lopes, E.N., Ehrhart, F. *et al.* (2020) WikiPathways: connecting communities. *Nucleic Acids Res.*, **49**, D613–D621.
- Oughtred, R., Stark, C., Breitkreutz, B.J., Rust, J., Boucher, L., Chang, C., Kolas, N., O'Donnell, L., Leung, G., McAdam, R. *et al.* (2019) The BioGRID interaction database: 2019 update. *Nucleic Acids Res.*, **47**, D529–D541.
- Orchard, S., Ammar, M., Aranda, B., Breuza, L., Briganti, L., Broackes-Carter, F., Campbell, N.H., Chavali, G., Chen, C., del-Toro, N. *et al.* (2014) The MIntAct project—IntAct as a common curation platform for 11 molecular interaction databases. *Nucleic Acids Res.*, **42**, D358–D363.
- Rodchenkov, I., Babur, O., Luna, A., Aksoy, B.A., Wong, J.V., Fong, D., Franz, M., Siper, M.C., Cheung, M., Wrana, M. *et al.* (2020) Pathway Commons 2019 Update: integration, analysis and exploration of pathway data. *Nucleic Acids Res.*, **48**, D489–D497.
- Domingo-Fernández, D., Mubeen, S., Marin-Llao, J., Hoyt, C. and Hofmann-Apitius, M. (2019) PathMe: Merging and exploring mechanistic pathway knowledge. *BMC Bioinformatics*, **20**, 243.

42. Alanis-Lobato, G., Andrade-Navarro, M.A. and Schaefer, M.H. (2016) HIPPIE v2.0: enhancing meaningfulness and reliability of protein-protein interaction networks. *Nucleic Acids Res.*, **45**, D408–D414.
43. Szklarczyk, D., Gable, A., Lyon, D., Junge, A., Wyder, S., Huerta-Cepas, J., Simonovic, M., Doncheva, N.T., Morris, J.H., Bork, P. et al. (2019) STRING v11: protein-protein association networks with increased coverage, supporting functional discovery in genome-wide experimental datasets. *Nucleic Acids Res.*, **47**, D607–D613.
44. Hagberg, A., Swart, P. and Chult, D.S. (2008) Exploring network structure, dynamics, and function using NetworkX. In: Varoquaux, G., Vaught, T. and Millman, J. (eds). *Proceedings of the 7th Python in Science conference (SciPy 2008)*. pp. 11–15.
45. Smyth, G.K. (2005) Limma: linear models for microarray data. In: *Bioinformatics and Computational Biology Solutions Using R and Bioconductor*. pp. 397–420.
46. Fisher, R.A. (1992) Statistical methods for research workers. In: *Breakthroughs in Statistics*. Springer, NY, pp. 66–70.
47. Benjamini, Y. and Yekutieli, D. (2001) The control of the false discovery rate in multiple testing under dependency. *Ann. Stat.*, **29**, 1165–1188.
48. Cassandri, M., Smirnov, A., Novelli, F., Pitolli, C., Agostini, M., Malewicz, M., Melino, G. and Raschella, G. (2017) Zinc-finger proteins in health and disease. *Cell Death Discov.*, **3**, 17071.
49. Gort, E.H., VanHaaften, G., Verlaan, I., Groot, A.J., Plasterk, R.H.A., Shvarts, A., Suijkerbuijk, K.P.M., van Laar, T., van der Wall, E., Raman, V. et al. (2008) The TWIST1 oncogene is a direct target of hypoxia-inducible factor-2 α . *Oncogene*, **27**, 1501–1510.
50. Peterson, T.R., Laplante, M., Thoreen, C.C., Sancak, Y., Kang, S.A., Kuehl, W.M., Gray, N.S. and Sabatini, D.M. (2009) DEPTOR is an mTOR inhibitor frequently overexpressed in multiple myeloma cells and required for their survival. *Cell*, **137**, 873–886.
51. Ratsada, P., Hijiya, N., Hidano, S., Tsukamoto, Y., Nakada, C., Uchida, T., Kobayashi, T. and Moriyama, M. (2020) DUSP4 is involved in the enhanced proliferation and survival of DUSP4-overexpressing cancer cells. *Biochem. Biophys. Res. Commun.*, **528**, 586–593.
52. Schmid, C.A., Robinson, M.D., Scheifinger, N.A., Müller, S., Cogliatti, S., Tzankov, A. and Müller, A. (2015) DUSP4 deficiency caused by promoter hypermethylation drives JNK signaling and tumor cell survival in diffuse large B cell lymphoma. *J. Exp. Med.*, **212**, 775–792.
53. Spencer, S.A., Suárez-Pozos, E., Escalante, M., Myo, Y.P. and Fuss, B. (2020) Sodium-calcium exchangers of the SLC8 family in oligodendrocytes: functional properties in health and disease. *Neurochem. Res.*, **45**, 1287–1297.
54. Gumulec, J., Raudenska, M., Adam, V., Kizek, R. and Masarik, M. (2014) Metallothionein-immunohistochemical cancer biomarker: a meta-analysis. *PLoS One*, **9**, e85346.
55. Frantseva, M.V., Fitzgerald, P.B., Chen, R., Möller, B., Daigle, M. and Daskalakis, Z.J. (2008) Evidence for impaired long-term potentiation in schizophrenia and its relationship to motor skill learning. *Cereb. Cortex*, **18**, 990–996.
56. Hasan, A., Nitsche, M.A., Rein, B., Schneider-Axmann, T., Guse, B., Gruber, O., Falkai, P. and Wobrock, T. (2011) Dysfunctional long-term potentiation-like plasticity in schizophrenia revealed by transcranial direct current stimulation. *Behav. Brain Res.*, **224**, 15–22.
57. Kristensen, A.S., Jenkins, M.A., Banke, T.G., Schousboe, A., Makino, Y., Johnson, R.C., Hagan, R. and Traynelis, S.F. (2011) Mechanism of Ca²⁺/calmodulin-dependent kinase II regulation of AMPA receptor gating. *Nat. Neurosci.*, **14**, 727–735.
58. Foster, W.J., Taylor, H.B., Padamsey, Z., Jeans, A.F., Galione, A. and Emptage, N.J. (2018) Hippocampal mGluR1-dependent long-term potentiation requires NAADP-mediated acidic store Ca²⁺ signaling. *Sci. Signal*, **11**, eaat9093.
59. Herring, B.E. and Nicoll, R.A. (2016) Long-term potentiation: from CaMKII to AMPA receptor trafficking. *Annu. Rev. Physiol.*, **78**, 351–365.
60. Qu, M., Tang, F., Wang, L., Yan, H., Han, Y., Yan, J., Yue, W. and Zhang, D. (2008) Associations of ATF4 gene polymorphisms with schizophrenia in male patients. *Am. J. Med. Genet. Part B: Neuropsychiatric Genet.*, **147**, 732–736.
61. Pasini, S., Corona, C., Liu, J., Greene, L.A. and Shelanski, M.L. (2015) Specific downregulation of hippocampal ATF4 reveals a necessary role in synaptic plasticity and memory. *Cell Rep.*, **11**, 183–191.
62. McInnes, L.A. and Lauriat, T.L. (2006) RNA metabolism and dysmyelination in schizophrenia. *Neurosci. Biobehav. Rev.*, **30**, 551–561.
63. Glatt, S.J., Cohen, O.S., Faraone, S.V. and Tsuang, M.T. (2011) Dysfunctional gene splicing as a potential contributor to neuropsychiatric disorders. *Am. J. Med. Genet. Part B: Neuropsychiatric Genet.*, **156**, 382–392.
64. Fan, Y., Abrahamson, G., McGrath, J.J. and Mackay-Sim, A. (2012) Altered cell cycle dynamics in schizophrenia. *Biol. Psychiatry*, **71**, 129–135.
65. Katsel, P., Davis, K.L., Li, C., Tan, W., Greenstein, E., Hoffman, L.B.K. and Haroutunian, V. (2008) Abnormal indices of cell cycle activity in schizophrenia and their potential association with oligodendrocytes. *Neuropsychopharmacology*, **33**, 2993–3009.
66. Pardo-Diaz, J., Bozhilova, L.V., Beguerisse-Diaz, M., Poole, P.S., Deane, C.M. and Reinert, G. (2021) Robust gene coexpression networks using signed distance correlation. *Bioinformatics*, btab041.
67. Piñero, J., Bravo, A., Queralt-Rosinach, N., Gutiérrez-Sacristán, A., Deu-Pons, J., Centeno, E., García-García, J., Sanz, F., Furlong, L.I. et al. (2016) DisGeNET: a comprehensive platform integrating information on human disease-associated genes and variants. *Nucleic Acids Res.*, **45**, D833–D839.
68. Hamosh, A., Scott, A.F., Amberger, J.S., Bocchini, C.A. and McKusick, V.A. (2005) Online Mendelian Inheritance in Man (OMIM), a knowledgebase of human genes and genetic disorders. *Nucleic Acids Res.*, **33**, D514–D517.
69. Peyvandipour, A., Saberian, N., Shafi, A., Donato, M. and Draghici, S. (2018) A novel computational approach for drug repurposing using systems biology. *Bioinformatics*, **34**, 2817–2825.
70. Rivas-Barragan, D., Mubeen, S., Bernat, F.G., Hofmann-Apitius, M. and Domingo-Fernández, D. (2020) Drug2ways: reasoning over causal paths in biological networks for drug discovery. *PLoS Comput. Biol.*, **16**, e1008464.
71. Fiscon, G. and Paci, P. (2021) SAveRUNNER: an R-based tool for drug repurposing. *BMC Bioinformatics*, **22**, 150.
72. Fiscon, G., Conte, F., Farina, L. and Paci, P. (2021) SAveRUNNER: a network-based algorithm for drug repurposing and its application to COVID-19. *PLoS Comput. Biol.*, **17**, e1008686.